Monthly Notices
of the
ROYAL ASTRONOMICAL SOCIETY

Mon. Not. R. Astron. Soc. **425,** 1357–1370 (2012) doi:10.1111/j.1365-2966.2012.21550.x

Multiwavelength intraday variability of the BL Lacertae S5 0716+714

Alok C. Gupta,[1⋆] T. P. Krichbaum,[2] P. J. Wiita,[3] B. Rani,[1,2] K. V. Sokolovsky,[2,4,5] P. Mohan,[6] A. Mangalam,[6] N. Marchili,[2] L. Fuhrmann,[2] I. Agudo,[7,8] U. Bach,[2] R. Bachev,[9] M. Böttcher,[10] K. E. Gabanyi,[11,12] H. Gaur,[1] K. Hawkins,[10] G. N. Kimeridze,[13] O. M. Kurtanidze,[13] S. O. Kurtanidze,[13] C.-U. Lee,[14] X. Liu,[15] B. McBreen,[16] R. Nesci,[17] G. Nestoras,[2] M. G. Nikolashvili,[13] J. M. Ohlert,[18,19] N. Palma,[10] S. Peneva,[9] T. Pursimo,[20] E. Semkov,[9] A. Strigachev,[9] J. R. Webb,[21] H. Wiesemeyer[7] and J. A. Zensus[2]

[1]*Aryabhatta Research Institute of Observational Sciences (ARIES), Manora Peak, Nainital 263 129, India*
[2]*Max-Planck-Institut für Radioastronomie (MPIfR), Auf dem Hügel 69, D-53121 Bonn, Germany*
[3]*Department of Physics, The College of New Jersey, PO Box 7718, Ewing, NJ 08628, USA*
[4]*Astro Space Center of Lebedev Physical Institute, Profsoyuznaya 84/32, 117997 Moscow, Russia*
[5]*Sternberg Astronomical Institute, Moscow State University, Universitetsky pr. 13, 119991 Moscow, Russia*
[6]*Indian Institute of Astrophysics, Sarjapur Rd, Koramangala, Bangalore 560 034, India*
[7]*Instituto de Astrofísica de Andalucía, CSIC, Apartado 3004, 18080 Granada, Spain*
[8]*Institute for Astrophysical Research, Boston University, 725 Commonwealth Avenue, Boston, MA 02215, USA*
[9]*Institute of Astronomy, Bulgarian Academy of Sciences, 72 Tsarigradsko Shosse Blvd., 1784 Sofia, Bulgaria*
[10]*Astrophysical Institute, Department of Physics and Astronomy, Ohio University Athens, OH 45701, USA*
[11]*FÖMI Satellite Geodetic Observatory, PO Box 585, 1592 Budapest, Hungary*
[12]*Konkoly Observatory, Research Centre for Astronomy and Earth Sciences, Hungarian Academy of Sciences, Konkoly Thege Miklos ut 15-17, Budapest 1121, Hungary*
[13]*Abastumani Observatory, Mt. Kanobili, 0301 Abastumani, Georgia*
[14]*Korea Astronomy and Space Science Institute (KASI), Daejeon 305-348, Republic of Korea*
[15]*Xinjiang Astronomical Observatory, the Chinese Academy of Sciences, 150 Science 1-Street, Urumqi 830011, China*
[16]*UCD School of Physics, University College Dublin, Dublin, Ireland*
[17]*Department of Physics, University La Sapienza, P. le Aldo Moro 2, I-00185 Roma, Italy*
[18]*Astronomie Stiftung Trebur, Fichtenstrasse 7, 65468 Trebur, Germany*
[19]*University of Applied Sciences, Wilhelm-Leuschner-Strasse 13, 61169 Friedberg, Germany*
[20]*Nordic Optical Telescope, E-38700 Santa Cruz de La Palma, Santa Cruz de Tenerife, Spain*
[21]*SARA Observatory, Florida International University, Miami, FL 33199, USA*

Accepted 2012 June 19. Received 2012 June 15; in original form 2012 March 15

ABSTRACT

We report results from a one-week multiwavelength campaign to monitor the BL Lacertae object (BL Lac) S5 0716+714 (on 2009 December 9–16). Nine ground-based telescopes at widely separated longitudes and one space-based telescope aboard the *Swift* satellite collected optical data. Radio data were obtained from the Effelsberg and Urumqi observatories and X-ray data from *Swift*. In the radio bands, the source shows rapid [$\sim$(0.5–1.5) d] intraday variability with peak amplitudes of up to $\sim$10 per cent. The variability at 2.8 cm leads by about 1 d the variability at 6 and 11 cm. This time lag and more rapid variations suggest an intrinsic contribution to the source's intraday variability at 2.8 cm, while at 6 and 11 cm, interstellar scintillation (ISS) seems to predominate. Large and quasi-sinusoidal variations of $\sim$0.8 mag were detected in the *V, R* and *I* bands. The X-ray data (0.2–10 keV) do not reveal significant variability on a 4 d time-scale, favouring reprocessed inverse Compton over synchrotron radiation in this band. The characteristic variability time-scales in radio and optical

⋆E-mail: acgupta30@gmail.com

bands are similar. A quasi-periodic variation of 0.9–1.1 d in the optical data may be present, but if so it is marginal and limited to 2.2 cycles. Cross-correlations between radio and optical bands are discussed. The lack of a strong radio–optical correlation indicates different physical causes of variability (ISS at long radio wavelengths, source intrinsic origin in the optical) and is consistent with a high jet opacity and a compact synchrotron component peaking at $\simeq$100 GHz in an ongoing very prominent flux-density outburst. For the campaign period, we construct a quasi-simultaneous spectral energy distribution, including γ-ray data from the *Fermi* satellite. We obtain lower limits for the relativistic Doppler boosting of $\delta \geq 12$–26, which for a BL Lac-type object is remarkably high.

Key words: galaxies: active – BL Lacertae objects: general – BL Lacertae objects: individual: S5 0716+714.

1 INTRODUCTION

Blazars are the extreme subset of active galactic nuclei (AGN) that are usually taken to include both BL Lacertae objects (BL Lacs) and flat spectrum radio quasars because both are characterized by rapid variability across the electromagnetic spectrum and significant radio to optical polarization. Their spectra are generally well modelled by synchrotron and inverse Compton (IC) emission from relativistic jets aligned nearly ($\lesssim 10^\circ$) with the line of sight (e.g. Urry & Padovani 1995). Blazar flux variations are seen on time-scales ranging from a few minutes through days and months to decades. Blazar variability time-scales can be divided into three classes: changes from minutes to less than a day are variously called microvariability, intranight variability, or intraday variability (IDV), which is the term we shall use; those from a few days to a few weeks are usually known as short time-scale variability (STV); flux changes from months to many years are called long-term variability (LTV; e.g. Gupta et al. 2004).

The vast majority of optical observations of blazars take place over single nights or several nights in succession at a given telescope, but these cannot provide the continuous coverage one would like to have in order to properly characterize and understand IDV and STV. The possibility that some coherent, even if temporary, fluctuations are present in blazar light curves is very important to investigate. Certainly one improves the chance of seeing such variations by having a long, densely sampled light curve. These requirements have led to several intensive campaigns in the past that have looked at individual blazars with multiple telescopes at widely separated longitudes over a few days through several months where simultaneous observations are obtained at different bands of the electromagnetic spectrum (e.g. Villata et al. 2000, 2006, 2008, 2009a,b; Raiteri et al. 2003, 2005, 2007, 2008a,b,c; Böttcher et al. 2005, 2009; Agudo et al. 2006; Ostorero et al. 2006; Fuhrmann et al. 2008; Larionov et al. 2008, and references therein).

We report results of a 7 d long multitelescope campaign on S5 0716+714 with a focus on IDV in the optical and at some radio bands. The campaign was conducted on 2009 December 9–16 with the most dense sampling and best frequency coverage during December 11–15. There have been many studies of this blazar, mainly in optical bands, since it is bright at a high declination and apparently always quite variable in the visible (e.g. Quirrenbach et al. 1991; Wagner et al. 1996; Sagar et al. 1999; Wu et al. 2005, 2007; Montagni et al. 2006; Stalin et al. 2006; Pollock, Webb & Azarnia 2007; Gupta et al. 2008; Poon, Fan & Fu 2009; Rani et al. 2010a, 2011; Chandra et al. 2011, and references therein). Our observing campaign also includes flux-density measurements made in the centimetre and millimetre radio, optical and X-ray bands.

Theoretical models that seek to explain optical IDV in AGN invoke several different mechanisms involving the accretion disc, including pulsation of the gravitational modes of the gaseous disc (e.g. Kato & Fukue 1980; Nowak & Wagoner 1992) or orbital signatures from 'hotspots' in the gas surrounding the black hole, either from the disc itself or the corona above it (e.g. Zhang & Bao 1991; Mangalam & Wiita 1993). However, for blazars, particularly in high states, the variability almost certainly arises within the Doppler-boosted relativistic jets and may well result from relativistic shocks in the jet (e.g. Marscher & Gear 1985) or turbulence behind such shocks (e.g. Marscher, Gear & Travis 1992; Marscher et al. 2008), from helical motion (e.g. Qian et al. 1991; Camenzind & Krockenberger 1992), instabilities (e.g. Hardee, Walker & Gomez 2005) or slight changes in viewing angles (e.g. Gopal-Krishna & Wiita 1992).

A key motivation of this campaign was to look for possible correlations between radio and optical variability. A positive correlation could substantially constrain the origin of the variability in the radio bands and would strongly favour an intrinsic origin over one due to interstellar scintillation (ISS; e.g. Simonetti, Cordes & Heeschen 1985; Rickett 1990). There have been earlier papers in which the variability properties of S5 0716+714 were discussed in both of these bands (e.g. Quirrenbach et al. 1991; Wagner & Witzel 1995; Wagner et al. 1996; Ostorero et al. 2006; Fuhrmann et al. 2008). Quirrenbach et al. (1991) reported correlated optical and radio variability in the source which, however, was not again seen in later observational campaigns. Optical variability was claimed to be associated with changes in the radio spectral index (Qian et al. 1995, 1996). This source is known to vary on different time-scales (IDV to STV to LTV) and has been claimed to exhibit quasi-periodic oscillations (QPOs) on all these time-scales. On IDV time-scales S5 0716+714 has shown QPOs on various occasions with time-scales ranging from $\sim$15 to 73 min (Gupta, Srivastava & Wiita 2009; Rani et al. 2010b). On STV time-scales, there is weak evidence for quasi-periodicity appearing on time-scales of $\sim$1 and $\sim$7 d (Quirrenbach et al. 1991; Wagner 1992; Heidt & Wagner 1996). On LTV time-scales, claims have been made for possible near periodicities of $\sim 3.0 \pm 0.3$ yr (Gupta et al. 2008). We adopt a redshift of $z = 0.31$ for this source (Nilsson et al. 2008) but the lack of spectral lines means that it is still quite uncertain (± 0.08).

In Section 2, we describe the observations and data reductions. We present our results in Section 3 and Section 4 includes a discussion and our conclusions.

2 OBSERVATIONS AND DATA REDUCTIONS

2.1 Radio data

The source S5 0716+714 was observed during 2009 December 11–15 with the Max-Planck-Institut für Radioastronomie (MPIfR) 100 m telescope at Effelsberg, Germany, and with the 25 m Nanshan radio telescope of the Urumqi Observatory, China. The observations and source selection at both observatories were coordinated and done in a similar manner. At Effelsberg, the observations were performed at three frequencies using the secondary focus heterodyne receivers operating at 2.7, 4.85 and 10.5 GHz. At Urumqi, the observations were done using a Cassegrain focus receiver, which operates at a frequency of 4.8 GHz. With both telescopes, the flux-density measurements were made in a similar way, with repeated cross-scans in azimuth and elevation. Frequent switching between target and calibrator sources on time-scales of a few minutes allowed us to monitor the gain variations introduced by the receiving system and the atmosphere. The gain variations seen in the calibrator sources were used to improve the flux-density calibration and correct for time and elevation dependences. This observing and calibration technique is well established and has been applied before for various IDV observations. The details of the observing strategy, the receiver parameters and the calibration methods have been described before (Gabányi et al. 2007; Fuhrmann et al. 2008; Marchili et al. 2010). As secondary calibrators, the two non-variable radio sources 0951+699 and 0836+710 were used. The absolute flux-density scale was set using 3C 286 and NGC 7027, adopting the scale of Zijlstra, van Hoof & Perley (2008).

2.2 Optical data

Our official campaign on S5 0716+714 began on 2009 December 11 and ran through 2009 December 15. Additional data were obtained on December 9, 10, 16 and 17, though the coverage was not as dense. We briefly describe the telescopes and cameras that were involved in these observations. We note that as this source is point-like, the different apertures used at different telescopes have negligible effects on the measured fluxes and agreement was excellent whenever different telescopes provided overlapping data.

The source was observed on 2009 December 12 with the 23.5 cm $f/10$ Schmidt–Cassegrain telescope located on the roof of the Department of Physics of La Sapienza University (Roma, Italy), with a Bessel *R* filter and a CCD camera with a Peltier cooled Kodak KAF 1603ME CCD chip. Due to the lack of a guiding system, images were taken in sequences of 9 to 10 frames with 60 s exposures and then stacked and summed together to increase the signal-to-noise ratio (S/N). Sky flats were used for flat fielding. Data reduction and analysis were performed with standard Image Reduction and Analysis Facility (IRAF)[1] routines. Aperture photometry was made with a 3.3 arcsec (2 pixels) radius. Simultaneous observations were made with the 31 cm $f/4.5$ Newtonian telescope located at Greve in Chianti (near Florence, Italy) equipped with a CCD camera with a back-illuminated Peltier cooled Site SIA502A chip and *B*, *V*, *R* and *I* Bessel filters. A four-colour sequence was made at the beginning of observations and then *R* filter monitoring began with 180 s exposure time. IRAF standard tasks were used for data reduction and analysis; aperture photometry was made with a 7 arcsec (2 pixels) radius. Photometric errors were estimated from the rms deviations of the reference stars, and found to be generally less than 0.01 mag. The light curves of the two instruments were in very good agreement. Reference standard stars were taken from Villata et al. (1998) in the same blazar field.

At the MDM Observatory on the south-west ridge of Kitt Peak, Arizona, USA, data were taken for limited periods during the nights of December 9, 10, 11 and 12 with the 1.3 m McGraw-Hill Telescope, using the Templeton CCD with *B*, *V*, *R* and *I* filters. The standard data reduction, using IRAF, included bias subtraction and flat-field division. Instrumental magnitudes of S5 0716+714 plus four comparison stars in the field (Villata et al. 1998) were extracted using the IRAF package DAOPHOT[2] (Stetson 1987) with an aperture radius of 6 arcsec and a sky annulus between 7.5 and 10 arcsec.

The observations at the Abastumani Observatory were conducted on 2009 December 9, 11, 12, 14, 15 and 16 at the 70 cm meniscus telescope ($f/3$). These measurements were made with an Apogee CCD camera Ap6E (1K × 1K, 24 μm^2 pixels) through a Cousins *R* filter with exposures of 60–120 s. Reduction of the image frames was done using DAOPHOT II. An aperture radius of 5 arcsec was used for data analysis.

Observations of S5 0716+714 were carried out on 2009 December 13 using the 50/70 cm Schmidt telescope at Rozhen National Astronomical Observatory, Bulgaria. The telescope is equipped with a FLI ProLine PL16803 CCD (4096 pixels × 4096 pixels), *BV* Johnson and *RI* Cousins filters. Standard data reduction used MIDAS and included bias subtraction and flat-field division. Instrumental magnitudes of S5 0716+714 and comparison stars in the field (Villata et al. 1998) were extracted using the MIDAS package DAOPHOT with an aperture radius of 5.6 arcsec (two times full width at half-maximum (FWHM)].

Observations of the source on 2009 December 11, 13 and 15 were carried out using the 1.04 m Sampurnanand telescope located at Nainital, India. It has Ritchey–Chretien optics with a $f/13$ beam equipped with a CCD detector which is a cryogenically cooled 2048 pixel × 2048 pixel chip mounted at the Cassegrain focus and Johnson *UBV* and Cousins *RI* filters. Each pixel of the CCD chip has a dimension of 24 μm^2, corresponding to 0.37 $arcsec^2$ on the sky, thereby covering a total field of ∼13 arcmin × 13 arcmin. Data processing (bias correction, flat-fielding and cosmic ray removal) was done by the standard routines in IRAF and photometry of the blazar and standard stars in its field employed a stand-alone version of DAOPHOT II. Aperture photometry was carried out with four concentric aperture radii, i.e. ∼1 × FWHM, 2 × FWHM, 3 × FWHM and 4 × FWHM. We found that aperture radii of 2 × FWHM almost always provided the best S/N, so we adopted that aperture for our final results.

Observations were also carried out on 2009 December 13 using the 61 cm Boller and Chivens reflector at Sobaeksan Optical Astronomy Observatory in Korea. The FLI CCD camera with thermoelectric cooled Kodak KAF 4301 2K CCD chip set and standard *R* Cousins filter were used for the observations. All images were reduced using standard IRAF tools. Aperture photometry parameters that maximized the S/N were an aperture radius of 1.5 × FWHM, an inner radius of the sky annulus of 5 × FWHM and a sky annulus width of 10 pixels.

On 2009 December 12, 13 and 14, the source was observed at the 1.2 m Cassegrain telescope at the Michael Adrian Observatorium of Astronomie Stiftung Trebur, Germany. A Roper Scientific EEV

[1] IRAF is distributed by the National Optical Astronomy Observatories, which are operated by the Association of Universities for Research in Astronomy, Inc., under cooperative agreement with the National Science Foundation.

[2] Dominion Astrophysical Observatory Photometry software.

1340 EB CCD camera and a Cousins *R* filter were employed. The data were reduced using MIRA PRO 7 software. An aperture radius of 2.9 arcsec, and inner and outer sky annulus radii of 10.4 and 13.8 arcsec, respectively, were used.

Observations of S5 0716+714 were carried out on 2009 December 12 at the 0.9 m optical SARA telescope at the Kitt Peak National Observatory, USA. The camera was an Apogee U42 with Johnson and Cousins *UBVRI* filter set. MIRA software was used for image processing and data analysis. The data were analysed with aperture size of 4 arcsec. The blazar light curve was calibrated using the local standard stars present in the blazar field (Villata et al. 1998).

The final set of ground-based optical observations of S5 0716+714 was carried out on 2009 December 10 and 16 at the 2.56 m Nordic Optical Telescope (NOT), Canary Islands, Spain, using ALOFSC (December 10) and MOSCA (December 16) using *UBVRI* filters. The data were reduced using standard IRAF procedures, including those for debiasing and twilight flat correction. The photometry was done using IRAF/APPHOT with the aperture radius chosen to be close to the FWHM of the image.

S5 0716+714 also was observed by the *Swift* satellite's Ultraviolet–Optical Telescope (UVOT; Roming et al. 2005) in the *V* band during 54 pointings conducted between 2009 December 11 and 15. The pointings were typically separated by the 96 min period of *Swift's* orbital revolution. Observations from the space-based platform have the obvious advantage of not being interrupted by the day/night cycle or unfavourable weather, and therefore can probe variability on time-scales of hours to days with dense and uniform sampling. The UVOT is a $D = 300$ mm, $f = 3810$ mm modified Ritchey–Chretien telescope equipped with a micro-channel plate-intensified CCD detector operated in photon counting (pc) mode. Detectors of this type may provide information about the time of arrival of individual photons and they have no specific saturation limit, but these advantages come at the cost of a non-linear response to the number of incoming photons because of the dead time after each registered photon event known as the coincidence loss (or pile-up) effect (Poole et al. 2008; Breeveld et al. 2010). The VAST software (Sokolovsky & Lebedev 2005) based on the SExtractor code (Bertin & Arnouts 1996) has been applied to conduct aperture photometry of the UVOT images. The VAST software is designed to deal with imaging data obtained with non-linear detectors (e.g. Kolesnikova et al. 2008, 2010) and has been successfully applied for the UVOT data reduction before (Sokolovsky 2009). The magnitude scale was set using comparison stars 4–8 from Villata et al. (1998). The data reduction technique we employed allows us to avoid uncertainties in the coincidence-loss correction for bright sources and enables direct comparison of the UVOT results with those obtained with ground-based telescopes after an $R-V$ colour correction of 0.43 ± 0.04 mag is applied (Rani et al. 2010a).

2.3 X-ray data

Swift's X-ray telescope (XRT; Burrows et al. 2005) observed the source simultaneously with the UVOT in the 0.2–10 keV energy range. The XRT was operating in the pc mode. The total exposure of 15.5 ksec was collected during 54 satellite pointings performed between 2009 December 11 and 15; each pointing was about 300 s long. Observations were processed using the `xrtpipeline` tool from the HEASOFT v6.8 package applying the standard filtering criteria. The mean count rate during the observations was 0.53 ± 0.01 cts/s which allows us to neglect the pile-up effect.

For the spectral analysis, all subexposures were combined into a single event file using `XSELECT`; the corresponding exposure maps were generated with `xrtexpomap` and combined using `XIMAGE`. The source spectrum was extracted from a circular region of 20 pixel radius. The background counts were extracted from a region away from the source. The auxiliary response file was generated with `xrtmkarf`, and the response matrix `swxpc0to12s6_20070901v011.rmf` was used. The spectrum was re-binned with the tool `grppha` to contain at least 25 counts per energy bin to enable the use of the χ^2 statistic. It was modelled with an absorbed power law, taking the neutral hydrogen column density fixed to the Galactic value of $N_{\rm H\,I} = 2.0 \times 10^{20}$ cm^{-2} from Kalberla et al. (2005) while the photon index, Γ, and the normalization were left as free parameters. The spectral modelling was conducted in XSPEC v12.5.1n.

For the light-curve analysis, the same procedure was applied to each individual subexposure. The value of Γ was fixed to that obtained from the combined spectrum to decrease the uncertainty of the flux measurements. Unabsorbed fluxes were computed by integrating the power-law model in the 0.2–10 keV energy range.

3 ANALYSIS AND RESULTS

3.1 Variability curves: general trends and behaviour

3.1.1 Radio

We characterize the variability parameters in the same way as in Fuhrmann et al. (2008), by the variability index, m, the noise-bias corrected variability amplitude, Y, and a reduced chi-square value, χ^2_r, for a fit to a constant flux.[3] In Table 1, we summarize the results. In column 1 we give the observing frequency, and in column 2 the mean flux density and its error. In column 3 the variability index of S5 0716+714 is given, while the next column contains the variability index of the secondary calibrators (0951+699 and 0836+710), which is a measure of the residual calibration errors. Column 5 has the variability amplitude Y, followed by the reduced χ^2_r in column 6, the number of measurements in column 7, the reduced χ^2_r value corresponding to a significance level of 99.9 per cent in column 8 and the observing telescope in the last column.

As is seen from Fig. 1, the overall variability is mild, with a decreasing trend of $\delta S/\langle S\rangle$ of $\sim$8 per cent at 2.7 and 4.8 GHz, and an $\sim$7 per cent increase in $\delta S/\langle S\rangle$ towards the end of the experiment at 10.5 GHz. At all frequencies, the source varies on time-scales of 0.5–1 d with a variability index m of about 1–2 per cent. Since the influence of the atmosphere and residual calibration errors increase with frequency, we also see a slight increase of the variability index of the secondary calibrators (m_0) with increasing frequency, from 0.25–0.33 per cent at 2.7 and 4.8 GHz to 1.1 per cent at 10.5 GHz. The calibration-bias corrected variability index Y takes into account the calibration uncertainties in m_0 and their frequency dependence. We therefore see a decrease of the variability amplitude Y for S5 0716+714 from 7 per cent at 2.7 GHz to 4.9 per cent at 10.5 GHz. Thus, the rms amplitude of the IDV of S5 0716+714 decreases with increasing frequency, as it could be expected for (weak) refractive ISS (e.g. Walker 1998, Beckert et al. 2002). We however note that our present finding is opposite to an observed increase of the variability amplitude with frequency for interday variability in this source when it was observed in 2003 November (Fuhrmann et al. 2008). Temporal changes of the frequency dependence of

[3] The source is considered to be variable if the χ^2-test gives a probability of $\leq$0.001 for the assumption of constant flux density.

Table 1. The variability analysis parameters at radio wavelengths.

Frequency GHz (cm)	Mean flux (Jy)	m (per cent)	m_0 (per cent)	Y (per cent)	χ^2_r	N	$\chi^2_{r\,99.9\,\mathrm{per\ cent}}$	Telescope
2.7 (11.0)	1.03 ± 0.024	2.35	0.30	7.0	63.595	127	1.44	Effelsberg
4.85 (6.0)	1.46 ± 0.024	1.67	0.25	4.94	24.360	132	1.44	Effelsberg
4.85 (6.0)	1.46 ± 0.029	2.01	0.33	5.94	16.256	117	1.45	Urumqi
10.5 (2.8)	2.45 ± 0.048	1.96	1.10	4.87	4.865	101	1.49	Effelsberg

m = variability index = $\sigma_S/\langle S\rangle$, σ_S standard deviation.
m_0 = variability index of the secondary calibrators.
$\mathrm{Y} = 3\sqrt{m^2 - m_0^2}$ = bias corrected variability amplitude (see Fuhrmann et al. 2008).
χ^2 = reduced Chi-square.
N = number of data points.
$\chi^2_{r\,99.9\,\mathrm{per\ cent}}$ = reduced Chi-square corresponding to a significance level of 99.9 per cent.

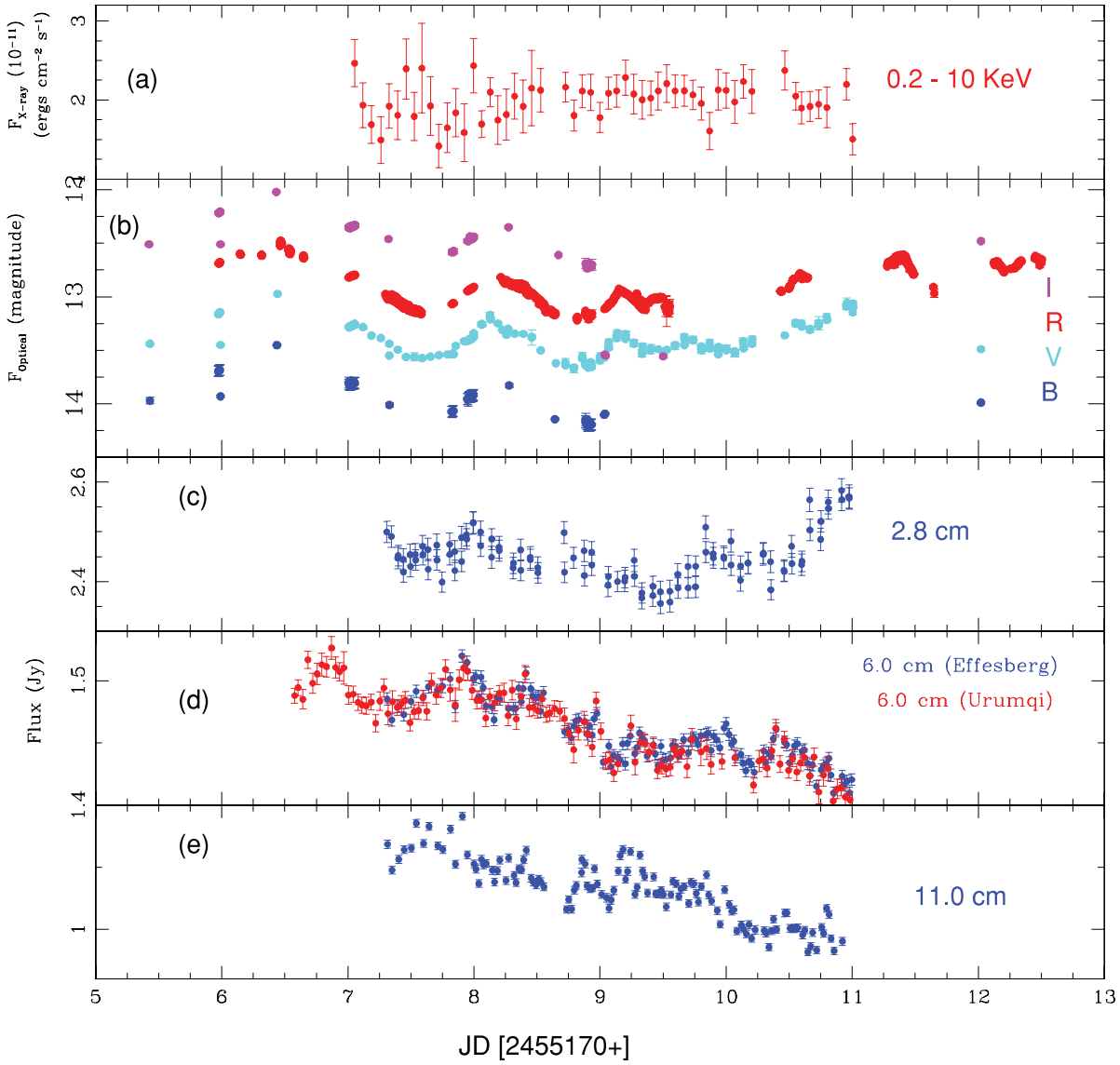

Figure 1. The broad-band (radio through optical to X-ray) variability observed in the source S5 0716+714 over the campaign period. (a) 0.2–10 keV light curve of the source; (b) optical light curves of the source in B, V, R and I passbands; (c) flux-density variability at 2.8 cm wavelengths; (d) the flux-density variability at 6.0 cm from two different telescopes (Effelsberg and Urumqi) and (e) flux-density variability at 11.0 cm wavelengths.

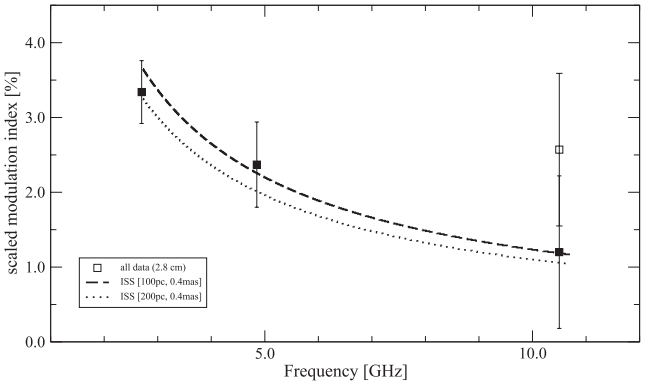

Figure 2. Variability index plotted versus frequency. At 10.5 GHz (2.8 cm), the open symbol is for the whole data set and the filled square represents the truncated data set without the flux density increase seen at the end (see the text). The lines show a model for a thin scattering screen located at a distance of 100 pc (dashed line) and 200 pc (dotted line).

the RADIO variability index in S5 0716+714 are well known and can be interpreted as a result of variable source size and the related change of the relative dominance of ISS over source intrinsic variability (cf. Krichbaum et al. 2002).

We qualitatively compare the observed modulation indices with those obtained from an analytical solution for the strength of ISS in the weak, quenched scattering regime (using equations of Beckert et al. 2002; see also Fuhrmann et al. 2008). For a plasma screen of 1 pc thickness and a turbulence strength similar to the value obtained from pulsar scintillation in the local bubble, the observed variability indices shown in Table 1 can be reproduced by assuming a scintillating component of size $\theta \sim 0.1$–0.2 mas [very long baseline interferometry (VLBI) core size at 5 GHz; Bach et al. 2006] and an adopted screen distance of ∼50–200 pc for the local bubble (Bhat, Gupta & Rao 1998). We further assume that the scintillating source component contains about 70 per cent of the source's total flux density as indicated from the VLBI compactness and re-scale the observed modulation indices accordingly. Fig. 2 shows the scaled and noise bias-corrected variability index ($\sim\sqrt{(m/0.7)^2 - m_0^2}$) plotted versus frequency together with models for screens at 100 and 200 pc distances. The data are in good agreement with this ISS slab model, which also reproduces the observed variability time-scale of the order of ∼1 d (see the following sections). At 10.5 GHz, however, the observed variability index is larger than expected from the model. At 4.8 GHz an annual modulation of the intra-day variability time scale has been found which is caused by ISS (Liu et al. 2012). Underlying source intrinsic variability may explain this excess. If we use only the first 2 d of the 2.8 cm data and by this omit the flux density rise seen at the end of the observations (see Fig. 1), the resulting lower variability index would agree with the expected frequency dependence (open and filled symbols in Fig. 2).

3.1.2 Optical

The variability is even more pronounced at optical frequencies. The optical light curves of the source in the *B*, *V*, *R* and *I* passbands shown in Fig. 1(b) display simultaneous flaring trends. Instead of a continuous rise or decay, multiple peaks and troughs of the flux were observed that give the appearance that the source might be showing nearly periodic variations. Although the *B*- and *I*-band light curves are less densely sampled compared to *V* and *R*, this behaviour is consistent through all the optical passbands. The variability time-scales are also comparable at all four optical passbands. Detailed discussions of the variability time-scales and a search for possible QPOs in the *R*-band light curve are given in Sections 3.2 and 3.6, respectively.

3.1.3 X-ray

While the source was highly active at optical frequencies, no significant variation of X-ray flux was detected during the campaign (see Fig. 1a). The χ_r^2 test returns a 0.75 probability that the entire observed light curve is the result of random noise. From the visual inspection of the light curve, it seems that in the beginning of the campaign (before JD 245 5178.6), the source exhibits some variations but it remains quiet during the second half of the campaign. The Kolmogorov–Smirnov (K-S) test gives only a 0.016 probability that flux measurements obtained before JD = 245 5178.6 and after this date are drawn from the same parent distribution. The χ_r^2 test returns a 0.58 probability that values before JD 245 5178.6 are just random noise while this rises to a 0.85 probability for the values after JD = 245 5178.6. It is possible that the object exhibits small IDV in X-rays, but we were not able to detect it significantly with these observations; the error bars are just too large.

3.2 Variability time-scales

To estimate any time-scale present in the variability at optical and radio wavelengths, we first employed the structure function (SF) analysis method. We followed Rani, Wiita & Gupta (2009) to calculate the SFs of the observed radio and optical light curves. Fig. 3 shows the SF for the three radio light curves at 11, 6 and 2.8 cm wavelengths. At 11 and 6 cm, the amplitude and time-scale of the variability are very similar, showing a break in the SF (indicating a characteristic variability time-scale) at $t_{\rm min} = 1.5 \pm 0.1$ d at 11 cm and $t_{\rm min} = 1.1 \pm 0.1$ d at 6 cm. The latter time-scale is visible in both the 6 cm data sets from Effelsberg and Urumqi. At 11 and 6 cm, another break near $t_{\rm max} = 2.9 \pm 0.1$ d is only marginally significant, since it is longer than half of the duration of the observations.

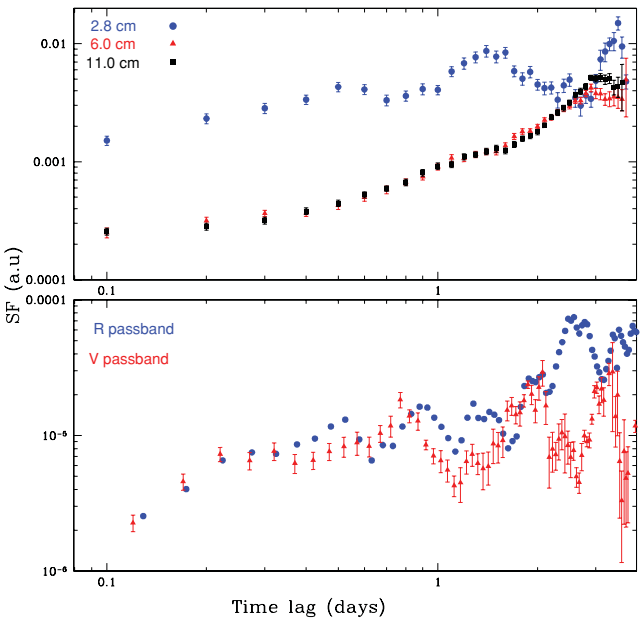

Figure 3. SF analysis curves of S5 0716+714, with radio in the upper panel and optical in the lower. Different symbols are used for different wavelengths.

For this slower variability ($t > 2.5-3$ d), the data indicate higher variability amplitudes at 11 cm than at 6 cm. The SF curves at 11 and 6 cm wavelengths are characterized by two different slopes. The SF curve at 11 cm follows a power-law slope, $\beta = 0.90 \pm 0.04$ until $t_{\rm min}$ (with $SF \propto t^{\beta}$) and then $\beta = 2.02 \pm 0.11$ from $t_{\rm min}$ to $t_{\rm max}$, while at 6 cm $\beta = 0.98 \pm 0.05$ until $t_{\rm min}$ and $\beta = 1.67 \pm 0.06$ from $t_{\rm min}$ to $t_{\rm max}$.

The SF of the data at 2.8 cm, however, shows a more pronounced and faster variability than for the two longer wavelengths. This is also seen in the auto-correlation functions (see Section 3.3 and Fig. 6). The characteristic time-scales of variability at 2.8 cm wavelength are $t_{\rm min} = 0.50 \pm 0.05$ d and $t_{\rm min} = 1.4 \pm 0.1$ d and the SF curve is characterized by a slope $\beta = 0.65 \pm 0.06$ until $t_{\rm min}$ and $\beta = 1.37 \pm 0.17$ from $t_{\rm min}$ to $t_{\rm max}$. Below $t \approx 3$ d, the variability at 2.8 cm appears more pronounced than that at 11 and 6 cm. However, Table 1 shows that the measurement uncertainty m_0 at 2.8 cm is 1.1 per cent, which is three to four times higher than at 11 or 6 cm. Although the formal significance of variability at 2.8 cm is higher than 99.9 per cent, the larger measurement uncertainty at this wavelength should lead to a cautious interpretation of the variability in this band. While in the first half of the 2.8 cm light curve the variability is very low ($m = 1.15$ per cent), we note in the second half a continuous rising trend in flux density, which is the main reason for the high significance of the overall variability. Since a departure from this rising trend is not seen, the true variability amplitude could be higher and the variability time-scale could be longer than 1.4 d.

In summary, we find that the fastest and most pronounced variability is seen at the shortest radio wavelength (2.8 cm) with a characteristic time-scale of 0.5 ± 0.05 d. Common to the three radio data sets (11, 6 and 2.8 cm) is also a slower variability mode, which appears at a characteristic time-scale of 1.1 d at 6 cm and to 1.4–1.5 d at 11 and 2.8 cm. The SF at 2.8 cm differs substantially from the more similar ones seen at 6 and 11 cm. Such different shapes towards higher frequencies were also seen previously in this source (Fuhrmann et al. 2008) and were interpreted as an indication for the presence of physically different variability mechanisms, as for example ISS dominating at the longer wavelength and with a frequency increasing contribution of source intrinsic variability. In this context, variability time-scales which are seen in the 2.8 cm data, but are not seen in the 11 and 6 cm data, may be related to some source intrinsic variability and may well therefore also appear in the optical, which is not affected by ISS.

In the optical bands, S5 0716+714 also displayed remarkable variability during the campaign period. The most dense coverage at optical frequencies was obtained in the *V* and *R* passbands. The SFs of these data are shown in Fig. 3. They show rapid variability with multiple cycles of rises and declines. Differences between both SFs are likely due to the different time sampling in both data sets and the location of observing gaps within the two data trains. The *B*- and *I*-passband light curves are much sparser and so cannot reveal significant features in the SF analysis. We therefore focus on the SFs for *R* and *V* bands. The first break in both *R*- and *V*-band SF curves appears at a time-scale of $t_{\rm min} = 0.25 \pm 0.05$ d. At the *R* band, the SF shows pronounced maxima also at 0.50 ± 0.05, 0.90 ± 0.05, 1.4 ± 0.1 and 1.9 ± 0.1 d. At the *V* band, the variations are less rapid, with a dominant time-scale at 0.8 ± 0.05 and 1.9 ± 0.1 d. The 0.5 d and the 1.4 ± 0.1 d time-scales, seen in the *R* band, are not seen in the *V* band.

We note that these time-scales are within their measurement error factor of two multiples of each other, providing a hint of an underlying 0.25 d quasi-periodicity (QPO). We further note that at 2.8 cm, the shortest time-scale seen in the SF is 0.5 d, which is very close to the second harmonic of the optical variability. This might indicate some correlation between radio and optical bands. We check the possibility for such a correlation in Section 3.3. We investigate the possibility for QPOs being present in the optical data using other techniques in Section 3.6.

3.3 Auto- and cross-correlations

To quantify the correlation among the multifrequency light curves of the source during the campaign period, we computed the discrete auto- and cross-correlation functions (ACF, DCF) between different frequencies to search for possible time lags. We followed Edelson & Krolik (1988) and Lehar et al. (1992) to calculate the DCF with details given in Rani et al. (2009).

In Fig. 4, we plot the two ACFs of the 6 cm data from the Effelsberg and Urumqi telescopes. The differences seen in the shape of the two ACFs is explained by the different data quality from the two telescopes, with a higher S/N and smaller beam size (and therefore lower in beam confusion) at the larger telescope.

In Fig. 5, we show the DCF of the 6 cm data from the Effelsberg and Urumqi telescopes. S5 0716+714 was observed at both telescopes with very similar time sampling and time coverage. The high degree of correlation of the two data trains is obvious and

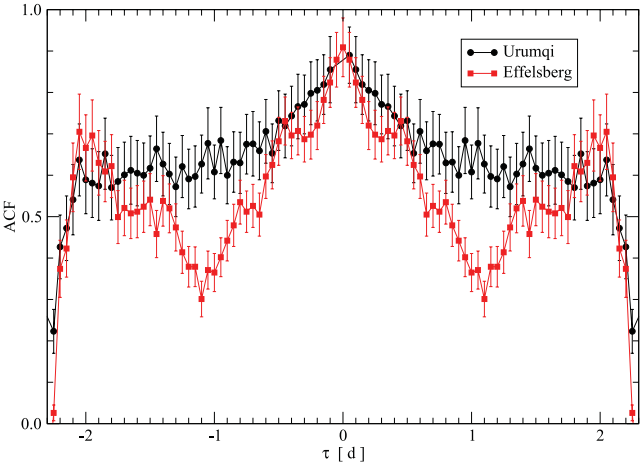

Figure 4. ACFs of the 6.0 cm data from Effelsberg and Urumqi.

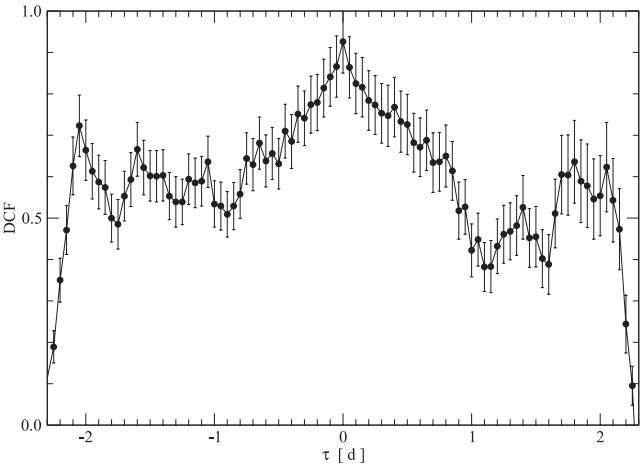

Figure 5. DCF of the 6.0 cm data between the Effelsberg and the Urumqi telescopes.

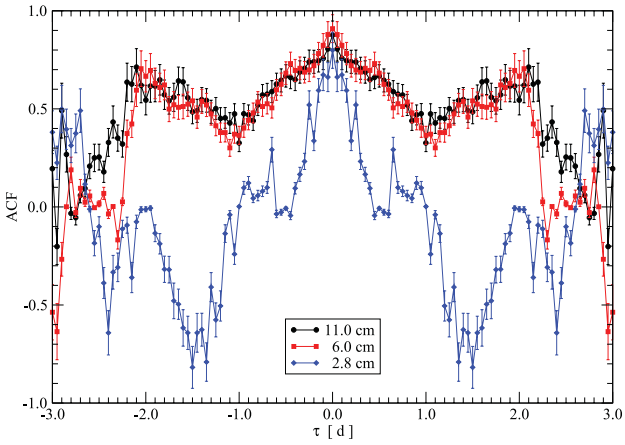

Figure 6. ACFs of the 11.0 cm (circles), 6.0 cm (squares) and 2.8 cm (diamonds) data from Effelsberg.

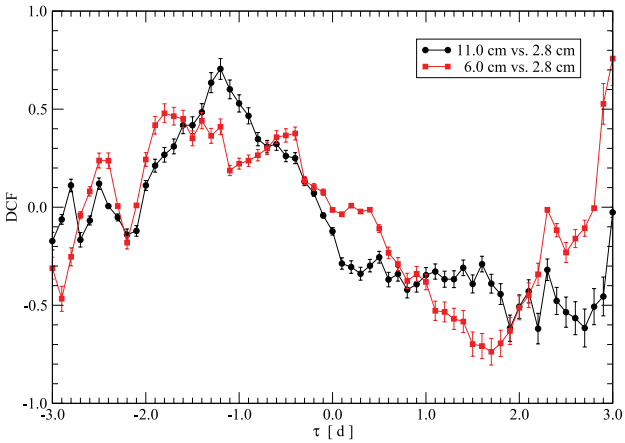

Figure 7. DCFs of the Effelsberg data: circles denote 11.0 versus 2.8 cm and squares denote 6.0 versus 2.8 cm.

convincingly demonstrate the reality of the observed IDV. No significant time lag ($\tau_{6.0/6.0} = 0.0 \pm 0.05$) is seen between the two telescopes.

Similar to the SF analysis (see Fig. 3), the ACFs of the 11 and 6 cm Effelsberg data show a common shape and show similar decorrelation time-scales (Fig. 6). On the other hand, the 2.8 cm data decorrelate much faster, indicative of faster variability at this shorter wavelength (higher frequency). The ACFs of the 11 and 6 cm bands also suggest a regular pattern on a ∼2 d time-scale. Since this time-scale is just half of the duration of the overall ∼4 d time coverage of the radio data, we do not regard this time-scale as significant.

To search for possible time lags between the three radio bands, we performed a cross-correlation analysis of the Effelsberg radio data. Fig. 7 shows the two independent cross-correlations of the 11.0 and 6.0 cm light curves versus the 2.8 cm data. Formally, we calculate a time lag of $\tau = -(1.2 \pm 0.1)$ d between 11.0 and 2.8 cm in the sense that the 2.8 cm data lead. Such frequency dependence is consistent with the canonical behaviour seen in AGN (e.g. van der Laan 1966, Marscher & Gear 1985).

Next, we look for a possible correlation with flux variations at optical–radio frequencies. Fig. 8 (top) may indicate a correlation with $\sim(0.35 \pm 0.15)$ d time lag between R and 2.8 cm, in the sense that radio is leading over optical, which apparently is opposite to physical expectations (the higher frequency should come first).

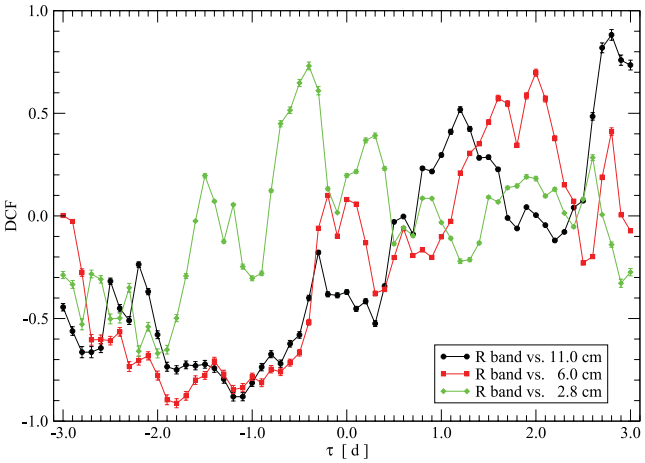

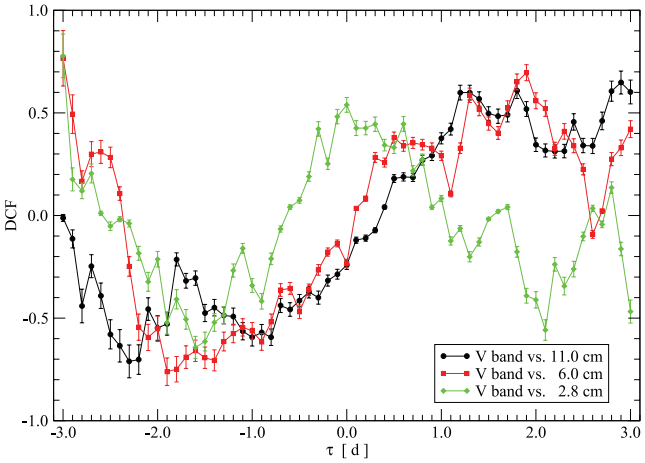

Figure 8. The cross-correlation analysis curves of the optical R-passband light curve (top) and the optical V-passband light curve (bottom) with all the three radio wavelength light curves of the source. A bin size of 0.1 d is used in the correlation analysis.

At the V band, the maximum correlation with 2.8 cm occurs at zero time lag, however, with a lower cross-correlation coefficient than for the R band (DCF peak at 0.73 for the R band and 0.53 for the V band). Since the R and V bands cross-correlate very strongly with zero time lag (Fig. 9), we think that the above time lag of ∼0.35 d is unlikely to reflect physical reality. The R-band light curve shown in Fig. 1 is less continuous and shows larger time gaps, while the V-band curve is more continuous and therefore better suited for the search of a possible cross-correlation. We generate flux–flux plots to quantify a possible correlation between optical and 2.8 cm data. In Fig. 10, we show the results using R-band data and in Fig. 11 using V-band data. Formally, we obtain the following correlation coefficients (r being the linear Pearson correlation coefficient) and significances. From Fig. 10, R versus 2.8 cm: $r = 0.163$ and 58.59 per cent significance; R versus time shifted 2.8 cm: $r = 0.687$ and 99.90 per cent significance. From Fig. 11, V versus 2.8 cm: $r = 0.52$ and 99.92 per cent significance. However, if we remove the highest data point in Figs 10 and 11, the correlation significance drops below 95 per cent for the R band versus 2.8 cm while it is still sustained for V versus 2.8 cm.

We therefore conclude that we cannot claim a significant detection of a correlation between the optical R band and the 2.8 cm radio

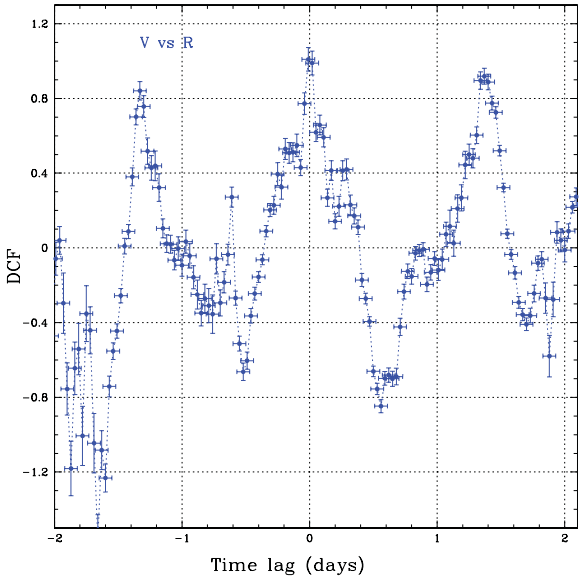

Figure 9. Cross-correlation analysis curves between the optical *V*- and *R*-band light curves. Although a bin size of 0.01 d is used in the correlation analysis this curve is shown with a bin size of 0.02 d.

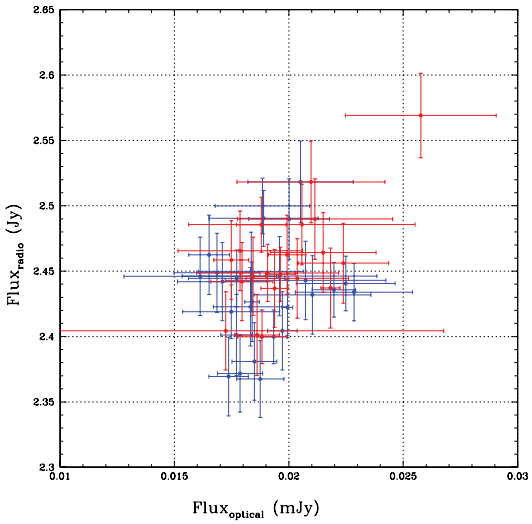

Figure 10. The 2.8 cm radio flux plotted versus optical *R*-band flux. The blue symbols show the original data, the time-shifted 2.8 cm radio data are shown in red (a 0.35 d shift was applied, see the text).

band, probably due to the limited time sampling of the *R*-band data. In the more continuous *V* band, however, such a correlation may exist, although we regard the evidence for it as weak and the nominal time lag as physically unlikely.

3.4 Spectral energy distribution

From the available multifrequency data of this campaign, we can construct a quasi-simultaneous spectral energy distribution (SED) of the BL Lac S5 0716+714. For the SED, we averaged in time all flux-density measurements obtained at the different observatories during the period 2009 December 11–15. For radio through X-ray bands, the length of the error bar reflects the strength of the variability. At GeV frequencies the error bars are derived from the spectral fitting. As the IDV observations were carried out only at

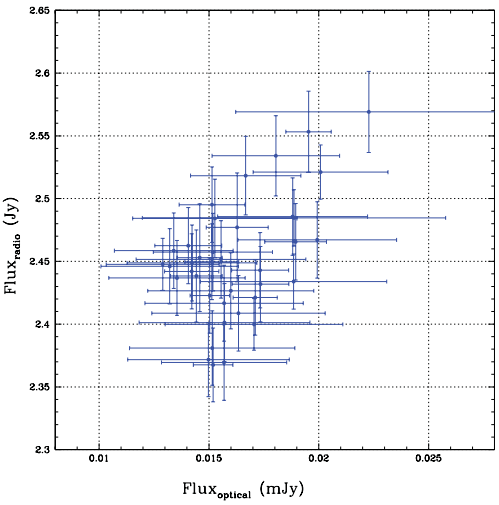

Figure 11. The 2.8 cm radio flux plotted versus the optical *V*-band flux.

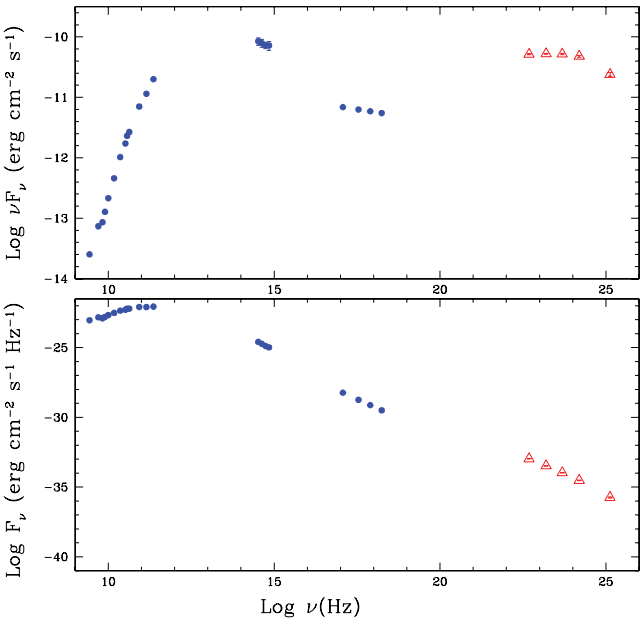

Figure 12. Broad-band (radio to γ-ray) spectrum of S5 0716+714 over the campaign period. Simultaneous data are in blue colour. For comparison, we also include the non-simultaneous γ-ray data from *Fermi*/LAT from the 2FGL catalogue (red symbols, see the text). The top panel shows the spectral energy (νF_ν), and the bottom panel shows flux density (F_ν) plotted versus frequency. For the radio through X-ray bands, the error bars represent here the variations in flux density rather than the measurement uncertainty.

three radio wavelengths, we also included additional flux-density measurements at other wavelength from IRAM and some public resources. These measurements were obtained quasi-simultaneously during the period 2009 December 9–16 and will be discussed in more detail in a forthcoming paper on the LTV of S5 0716+714 (Rani et al., in preparation).

The SED of the source is displayed in Fig. 12. The upper panel displays the $\nu - \nu F_\nu$ plot, while the $\nu - F_\nu$ plot is shown in the lower panel. The maximum luminosity of the SED appears to be in the range of around 10^{12}–10^{14} Hz, which unfortunately is in a spectral region with no data.

In the SED, we also included the public available γ-ray data from the second AGN catalogue of the *Fermi* satellite (2FGL catalogue;

Ackermann et al. 2011). These data result from a 2-year average (2008–2010 August) of the source flux density and therefore are not truly simultaneous with our observing campaign. We note however that S5 0716+714 was in a low γ-ray state at the time of our observation, so the expected GeV fluxes in 2009 December are likely be lower than the 2FGL catalogue values plotted in this SED.

3.5 Jet Doppler factors

Within the framework of synchrotron self-Compton models, it is possible to constrain the IC Doppler factor ($\delta_{\rm IC}$) by comparing the expected and observed fluxes at higher frequencies (Marscher 1987; Ghisellini et al. 1993). This IC Doppler factor is defined as

$$\delta_{\rm IC} \geq f(\alpha) S_m \left(\frac{\ln(\nu_b/\nu_m)\nu_\gamma^\alpha}{S_{\rm IC}\theta_\nu^{(6-4\alpha)}\nu_m^{(5-3\alpha)}} \right)^{1/(4-2\alpha)} (1+z), \quad (1)$$

where ν_b is the synchrotron high-frequency cut-off in GHz, S_m the flux density in Jy at the synchrotron turnover frequency ν_m, $S_{\rm IC}$ the observed γ-ray flux in Jy (assumed to arise from the IC process) at ν_γ in keV, α is the spectral index of the optically thin part of the spectrum, θ_ν the angular source size in milliarcsec and $f(\alpha) \simeq 0.14 - 0.08\alpha$. For the high-energy cut-off, we follow Fuhrmann et al. (2008) and use $\nu_b \sim 5.5 \times 10^5$ GHz. The angular size of the rapidly varying region θ_ν is constrained to be $\leq$0.03 mas as used by Agudo et al. (2006) and consistent with size measurements from millimetre VLBI. We adopt this value in our further calculations. For the radio spectrum, we use an optically thin spectral index of $\alpha = -0.44$, and for the synchrotron turnover we adopt $S_m = 8.9$ Jy and $\nu_m = 148$ GHz (for details of spectral fitting see Rani et al., in preparation).

The estimated limits on $\delta_{\rm IC}$ are 18.8 (adopting $S_{\rm IC} = 1.77 \times 10^{-6}$ Jy at $\nu_\gamma = 1.4$ keV) and $\delta_{\rm IC} = 26.1$ (adopting $S_{\rm IC} = 1.73 \times 10^{-7}$ Jy at $\nu_\gamma = 7.2$ keV). If the same calculation is applied for the GeV fluxes and if we assume that the same photons would also be producing the γ-rays, then a considerably higher Doppler factor of $\delta_{\rm IC} = 69$ is obtained (adopting $S_{\rm IC} = S_\gamma = 1.95 \times 10^{-11}$ Jy at $\nu_\gamma = 5.47 \times 10^5$ keV).[4] For a given Lorentz factor γ, the maximum Doppler factor is $\sim 2\gamma$. A Doppler factor of up to $\sim$50 therefore is consistent with the observed jet speed, which is in the range of $\gamma =$ 15–25 (Bach et al. 2005; Fuhrmann et al. 2008; Rastorgueva et al. 2009).

In the IC process, it is usually assumed that the synchrotron photons from the infrared–optical branch are scattered up to GeV energies. If we assume that the jet is not stratified, i.e. that the Doppler boosting is homogeneous over the emission region, we find that the observed GeV flux could also be explained via IC scattering from a synchrotron component with a spectral maximum in the 300–400 GHz regime. The possibility of SSC dominance in Compton dominated blazars has been investigated in detail in Zacharias & Schlickeiser (2012).

It is also possible to obtain a limit on the Doppler factor δ by assuming that the high-energy γ-ray photons can collide with the softer radiation to produce $e^\pm$ pairs. The cross-section of this process is maximized at $\sim\sigma_{\rm T}/5$ (see Svensson 1987 for details), where $\sigma_{\rm T}$ is the Thompson scattering cross-section. This leads to a lower limit on δ (following Dondi & Ghisellini 1995):

$$\delta \geq \left[3.5 \times 10^3 \frac{(1+z)^{2\alpha}(1+z-\sqrt{1+z})^2 F_{\rm x}(3.8\nu\nu_{\rm x})^\alpha}{t_{\rm var}} \right]^{1/(4+2\alpha)}, \quad (2)$$

where $F_{\rm x}$ is the X-ray flux in μJy and $\nu_{\rm x}$ is the corresponding X-ray frequency in keV, ν is the GeV frequency, α is the spectral index measured between 1 keV and 100 MeV. Using $F_{\rm x} = 1.77$ μJy, $\nu_{\rm x} =$ 1.44 keV, $\alpha = -1.05$, we obtained $\delta \geq 24$ for 300 MeV and $\delta \geq 12$ for 1 GeV energies. Since the published GeV data are not simultaneous with our radio to X-ray data, the accuracy to which the Doppler factors can be estimated is limited. A more accurate, though not largely different, estimate of the Doppler boosting will be presented in a forthcoming paper, which is based on truly simultaneous γ-ray data (Rani et al., in preparation).

From all of the above approaches, we think it is reasonable to conclude that the blazar S5 0716+714 exhibits a high Doppler factor of at least 12 and most likely $\geq$20–25, which is not typical for a BL Lac-type object.

3.6 Nearly periodic variations in the optical?

The complete optical light curve is given in Fig. 13, with the different observatories labelled. It is important to note the excellent agreement between the data taken at different telescopes during the many periods when we had essentially simultaneous coverage. Over the course of the total seven days of these observations the *R* magnitude of S5 0716+714 varied between 12.48 and 13.25 mag. Strong variations were seen throughout the campaign, with frequent excursions of 0.2–0.4 mag over a few hours. Such changes are not uncommon for this active blazar (e.g. Montagni et al. 2006; Gupta et al. 2008; Rani et al. 2011, and references therein). The duty cycle in previous observations was found to be unity, with some detectable variation every time it is observed for more than a few hours (Wagner & Witzel 1995; Wagner et al. 1996) and our results certainly agree with those earlier data. We have quantified these variations by examining them for possible time-scales and quasi-periodic fluctuations.

Following Mohan et al. (in preparation), we employ a suite of statistical techniques to analyse the optical light curve (Fig. 11), namely Fourier periodogram, wavelet analysis, multiharmonic analysis of variance (MHAoV) and Lomb–Scargle periodogram (LSP). The LSP and MHAoV offer a natural way of period detection when the data are unevenly sampled with the MHAoV also able to detect non-sinusoidal signals. Together, these are designed to detect possible QPOs and test the validity of a detection using Monte Carlo (MC) simulation-based significance testing. This suite helps in making QPO detection reliable through consistent detection with significance testing in all techniques. In addition, the phase of existence and number of cycles a QPO is present during the entire length of the observations are obtainable from a wavelet analysis. As an example of this suite technique, we apply it to our new data on S5 0716+714.

The fitting of the Fourier periodogram (top plot in Fig. 14) follows the procedure described in Vaughan (2005). It is well fit by a power-law model with a slope of -2.0 ± 0.16. The K-S goodness of fit test yields a p value of 0.99 indicating a good fit. Errors on the fit parameters, the slope and normalization are determined. Then, the error on the power-law model is evaluated, after which model uncertainties are accounted for before placing a 99 per cent significance contour (top plot in Fig. 14). There are no significant detections above this level. MC simulations are carried out using the Timmer & König (1995) algorithm to generate 6600 random light curves with a range of slopes within the fit parameter errors to simulate the properties of the original light curve. The MHAoV and LSP are determined for each of the generated light curves and an estimate of the number of times the data-based MHAoV and LSP ordinates at

[4] The GeV fluxes were obtained from publicly available *Fermi*/LAT light curves at http://fermi.gsfc.nasa.gov/ssc/data/access/lat/msl_lc

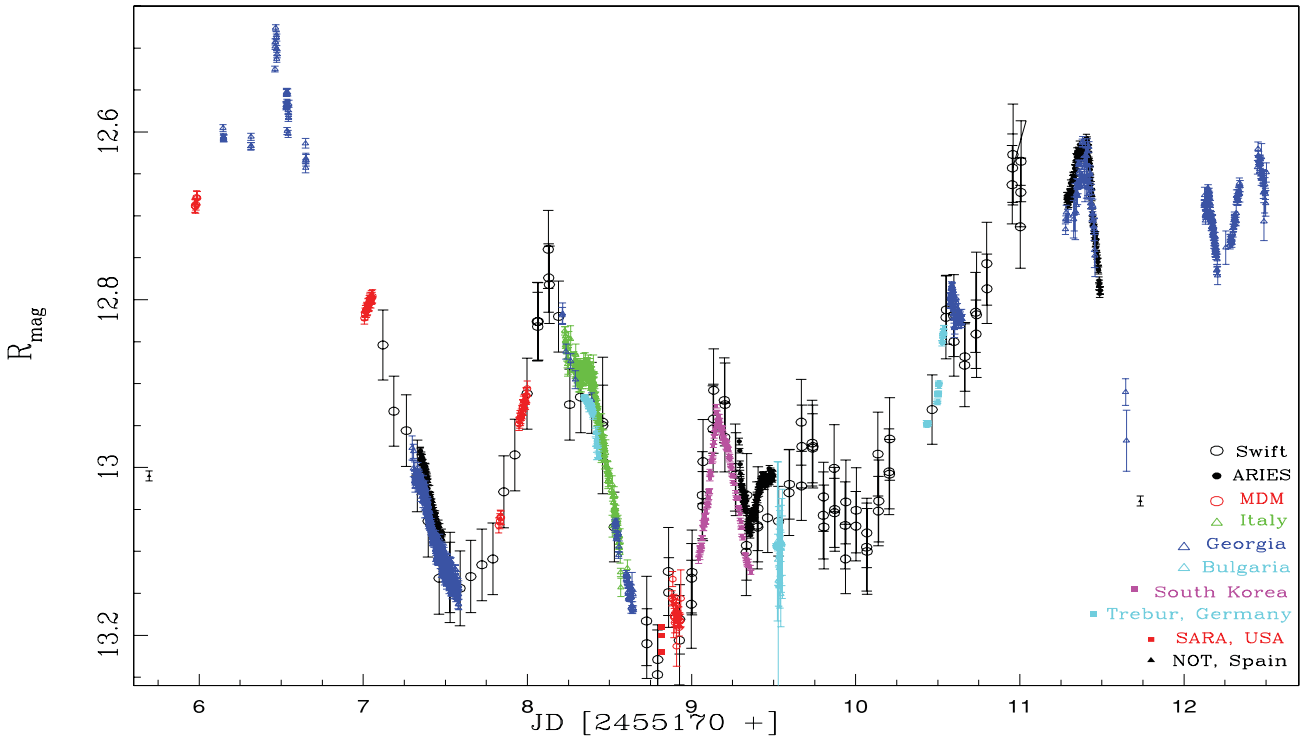

Figure 13. *R*-passband light curve of the blazar S5 0716+714. Different symbols and colours denote data from different observatories. Colour-corrected *V*-band data from *Swift* were added to complement the time coverage.

the interesting periodicity are above the simulated ordinates gives a measure of the significance. The MHAoV (bottom plot in Fig. 14) detects a possible period at 1.1 d with a probability of 94.6 per cent from the MC simulation-based significance test. The LSP (bottom plot in Fig. 14) detects the same period of 1.1 d with a probability of 80 per cent from the MC simulation-based significance test. The wavelet analysis (Fig. 15) indicates a quasi-period of $0.93^{+0.15}_{-0.28}$ d in the duration between ∼7.4 and 9.4 d within the cone of influence (triangular bounded region in between the two black lines in Fig. 15) indicating that it lasts for 2.2 cycles. By integration of the wavelet signal along the time axis (abscissa in Fig. 15), the global wavelet power spectrum (GWPS) is obtained (bottom plot of Fig. 14).

Since the nominal periodicity shows a fairly large range of 0.65–1.1 d in the optical data, and since it lasts only for 2–3 cycles, any periodicity that may be present is certainly broad and weak. We can argue that a time-scale of ∼1 d has been seen in the optical variations during our campaign as it is supported by the moderate significance estimated for the MHAoV and LSP detections. However, despite having a relatively large amount of optical data from telescopes at different longitudes, there were gaps during the campaign that were only filled in by the *Swift* UVOT monitor. These data are of lower accuracy than the bulk of the ground-based data and they affect the sensitivity of our tests for QPOs.

4 DISCUSSION AND CONCLUSIONS

We have successfully carried out a multiwavelength campaign to observe the well-known blazar S5 0716+714. The optical portion of the data that we have reported here was obtained from nine ground-based and one space-based telescopes over almost 7 d. The target was very active, with repeated 'mini-flares' of 0.2–0.7 mag in amplitude and an overall variability of 0.8 mag in the optical *V* band. Significant peak-to-peak variations of the order of 5–10 per cent were also seen in the radio bands but only marginal variability was detected in the X-rays. In the radio bands, the variability amplitudes increase with frequency and the variability time-scales become shorter. We find significant correlations between the different radio bands as well as between the optical passbands, but no significant correlations between radio/optical and X-ray bands.

The visual inspection of the optical light curve suggests the presence of a characteristic variability time-scale. Therefore, we analysed this formally using the periodogram, LSP, MHAoV and wavelet techniques. A time-scale in the range of 0.9–1.1 d is determined from these. Because of its moderate formal significance (80 per cent from LSP and 94.5 per cent from MHAoV analyses) and a small number of putative cycles (2.2 seen in the wavelet analysis) a formal claim of strict (or quasi-) periodicity cannot be made.

The SF analysis yields for the three fastest variability mode time-scales of 0.25, 0.5 and 1.0 d in the optical bands. In the radio bands, the three fastest variability modes appear at 0.5, 1.1 and 1.5 d. Within the measurements' uncertainties, the variability time-scales at 0.5 d and 1.0 d appear common between the radio and optical bands. It may be noteworthy that these time-scales are essentially integer multiples of the fastest optical variability time-scale of 0.25 d. It is unclear whether this is a chance coincidence or reflects a common physical origin.

A comparison of the observed modulation indices at radio bands with the expected strength for (weak) ISS suggests that most of the observed radio IDV is in agreement with an ISS slab model, which is able to reproduce the observed variability time-scale of the order of ∼1–2 d. At 2.8 cm, however, the observed variability index is larger than expected from the model which could be due to some 'underlying' source intrinsic variability. This interpretation is supported by the detection of a time lag between 2.8 cm and the

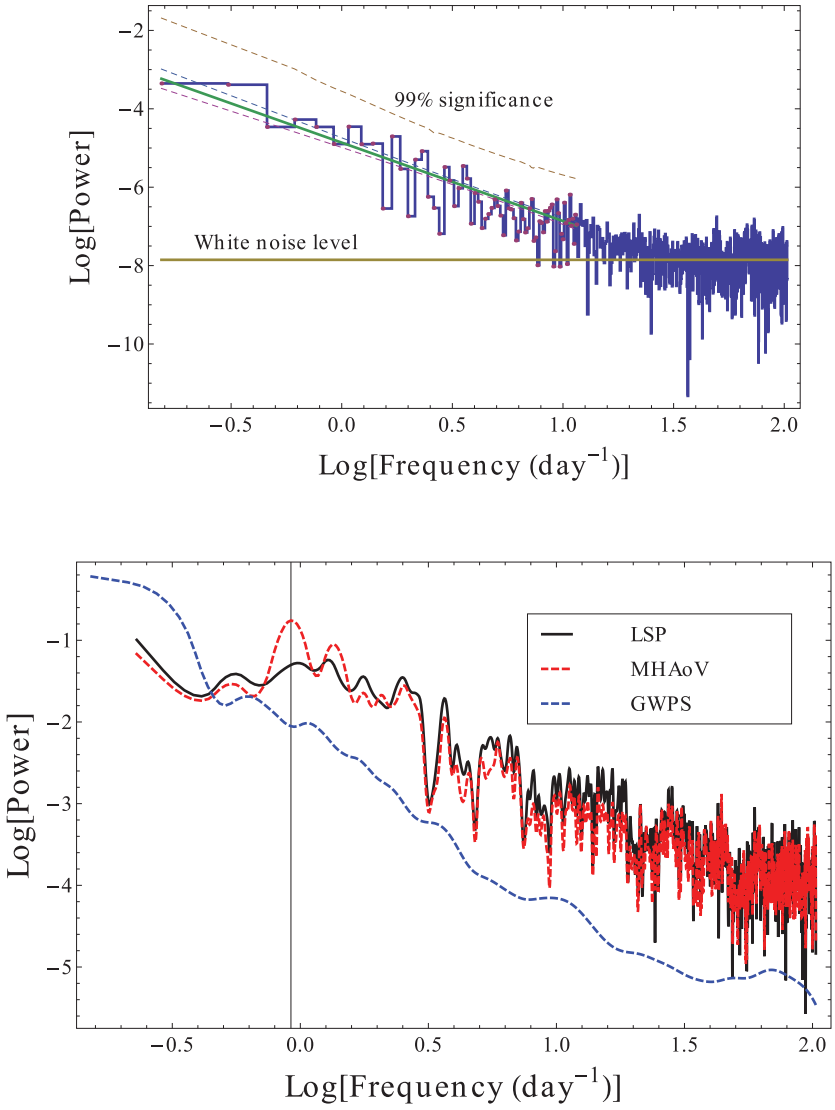

Figure 14. Top plot: periodogram on a log–log scale. The yellow solid line indicates the white noise level which is the contribution of photon shot noise at all frequencies. The green solid line indicates the best-fitting power law to the log–log periodogram. The dashed lines above and below the best-fitting line indicate the errors on the power-law model. The upper yellow dashed line indicates the 99 per cent significance contour, taking into account errors on the power law as well as model uncertainties. Bottom plot: combined plot showing the LSP, MHAoV and the GWPS on a log–log scale with a black vertical line at the position of the periodicity of 1.1 d. The MHAoV and LSP indicate a feature at 1.1 d with significances of 94.6 and 80 per cent, respectively. The GWPS shows a minor feature at 0.93 d just to the right of this. All the curves are normalized such that the total power summed over all frequencies between the sampling and the Nyquist frequency is equalized.

longer wavelengths in the sense that the 2.8 cm variability is leading. This is typical for AGN variability and is commonly interpreted as a source intrinsic opacity effect.

We note a possible cross-correlation between the 2.8 cm and the optical *V* band. Although mathematically significant, such a correlation must be regarded with some skepticism in view of the lack of a similar correlation at the *R* band, the unexpected sign of the putative time lag (radio is leading) and the limited length of the data trains. So we cannot claim any significant correlation between the flux variations at optical and radio frequencies over this one-week IDV campaign. We further note that in their analysis of the LTV of S5 0716+714 during 2007–2011, in which S5 0716+714 shows a prominent flare with peak in late 2009 December, Rani et al. (in preparation) find that the optical flux variations lead the radio by ∼(60–70) d. Such a time lag would exclude any direct radio–optical correlation in the one-week-long data train discussed here.

As a matter of fact, correlated radio–optical variability of this source has been investigated in several earlier observing campaigns. During four weeks of multifrequency observations in 1990 February, Quirrenbach et al. (1991) detected a significant one-to-one correlation between optical/radio flux variability (see also Qian et al. 1996; Wagner et al. 1996). Such a correlation was not seen in two later radio–optical IDV campaigns, which were performed in 2000 (unpublished data) and in 2003 (Agudo et al. 2006; Ostorero et al. 2006; Fuhrmann et al. 2008).

To further explore the possibility of a radio–optical correlation, we examine the spectral characteristics of S5 0716+714 for three different radio-/optical-IDV campaigns. In Table 2, we summarize for each observing date the spectral properties of S5 0716+714, where we used flux densities averaged over the duration of the campaign. In the table, we list the synchrotron peak frequency ($\nu_{\rm max}$) in column 2, the radio spectral index in column 3 and the

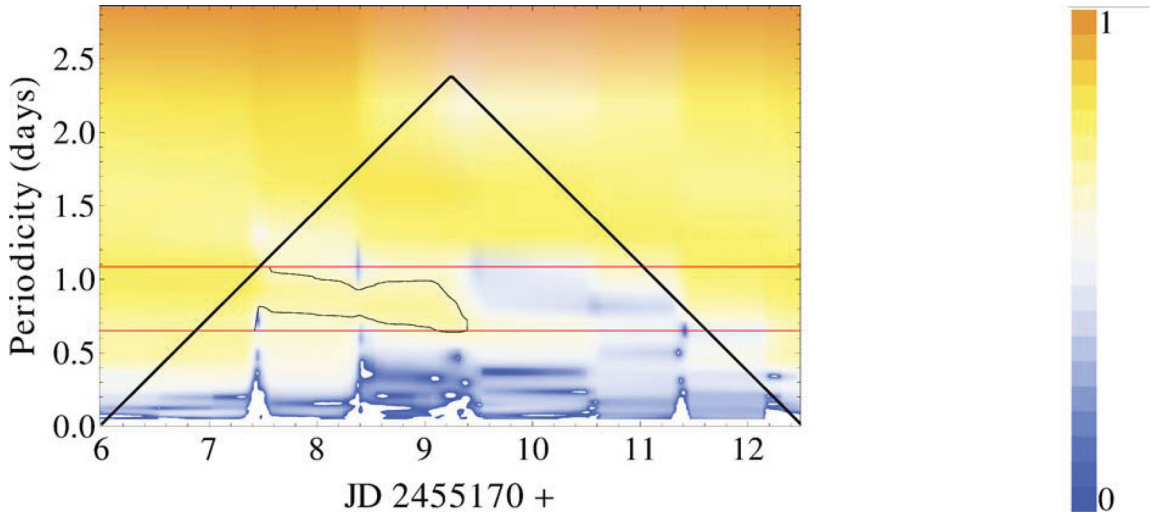

Figure 15. Wavelet contour plot beside which is an intensity scale indicating the colour scaling of the wavelet power. Contour plot abscissa: time duration of observation; ordinate: periodicities searched for in the detection of a quasi-periodic signal. A broad feature between JD 245 5170 + 7.4 and 9.4 d is indicated inside a contour drawn between periodicities of 0.65 and 1.08 d (horizontal red lines) within the cone of influence. This contour indicates the wavelet power above 90 per cent confidence in this region. A periodicity of $0.93^{+0.15}_{-0.28}$ is indicated which lasts for 2.2 cycles.

Table 2. A comparison of spectral variations over different campaign epochs.

Epoch	$\nu_{\rm max}$	$\alpha_{\rm radio}$	$\alpha_{\rm mm-optical}$	Reference
1990 February	35 ± 5	-0.82 ± 0.08	-0.75 ± 0.05	1
2003 November	90 ± 5	-0.35 ± 0.10	-0.88 ± 0.04	2
2009 December	114 ± 12	-0.44 ± 0.10	-0.85 ± 0.03	3

$\nu_{\rm max}$: synchrotron peak frequency in GHz from spectral fit.
$\alpha_{\rm radio}$: optically thin radio spectral index calculated by fitting a synchrotron self-absorbed model over a frequency range 2.7–230 GHz.
$\alpha_{\rm mm-optical}$: spectral index from 230 GHz to the optical *R* band.
Reference: (1) Quirrenbach et al. 1991; (2) Ostorero et al. (2006) and (3) this paper.

millimetre−optical spectral index in column 4. We see that in 1990, the source showed a factor of ∼3 lower synchrotron turnover and considerably steeper radio spectrum than in the later two campaigns, where S5 0716+714 was much more active and showed prominent flux-density outbursts.

It is therefore likely that the detection/non-detection of correlated radio–optical IDV relates to the activity state of the source. In particular, the opacity of the emitting region in the centimetre bands (e.g. Qian 2008) and the presence of high- or low-peaking flux-density flares, which trace moving shocks in a relativistic jet at different separations from the jet base (e.g. Valtaoja et al. 1992), may determine the presence of such correlations. Near and above the actual turnover frequency, the opacity decreases progressively, the spectrum steepens and the time lag between radio and optical variations vanishes. The direct radio–optical correlation seen in 1990 February implied a small (<1 d) time lag in the variability, which is fully consistent with the observed optically thin state and a time of intermittent quiescence in the overall source variability.

The detection of QPOs with similar time-scales in the radio and optical band would restrict their physical origin to jet rather than to accretion disc physics. As the activity state of the source and its time variable opacity play a fundamental role in the search for correlated radio–optical IDV, we see two ways to proceed in the near future: (i) observe during times of low activity, e.g. minimal flux and steep spectrum, and/or (ii) observe at frequencies above the critical turnover frequency, which for S5 0716+714 is at ≥100 GHz (in millimetre and submillimetre bands). In the optically thin regime, the lower source opacity will ensure that the observer actually looks at the same physical region. In order to facilitate the identification of QPOs, data trains have to be long enough in time so that a sufficiently large number of variability cycles can be observed. With a typical variability time-scale of 0.5–1.5 d in S5 0716+714, at least 5–10 duty cycles are necessary to unambiguously identify a QPO. This means that a continuous broad-band monitoring for more than one-week duration is necessary. In order to separate the intrinsic variability from unavoidable ISS (caused by the small size of the emission region), multifrequency observations are required, with a frequency coverage which should include the millimetre and submillimetre radio bands. This will help to avoid the effects from ISS, which dominate at the longer centimetre wavelengths.

ACKNOWLEDGMENTS

We thank the referee for constructive comments that have helped us to improve the paper. We acknowledge data from the 100 m Effelsberg radio telescope, which is operated by the Max-Planck-Institute für Radioastronomie in Bonn (Germany). This paper made use of the data obtained with the Urumqi 25 m radio telescope of Xinjiang Astronomical Observatory of the Chinese Academy of Sciences (CAS). The IRAM 30 m Telescope is supported by INSU/CNRS (France), MPG (Germany) and IGN (Spain). We thank the *Swift* team for making these observations possible. The work of ACG, BR, RB, HG, SP, ES and AS was partially supported by Scientific Research Fund of the Bulgarian Ministry of Education and Sciences (BIn-13/09 and DO 02-85) and by Indo Bulgaria bilateral scientific exchange project INT/Bulgaria/B-5/08 funded by DST, India. The work of PJW is partially supported by US NASA grant NNX11AB90G. The Abastumani Observatory team acknowledges financial support by the Georgian National Science Foundation through grant GNSF/ST09/521_4-320. The work of KÉG was partially supported by the COST Action MP0905 'Black Holes in

a Violent Universe' and by the Hungarian Scientific Research Fund (OTKA, grant no. K72515). IA acknowledges the funding support by the regional government of Andalucía, and by the Ministerio de Ciencia e Innovación of Spain through grants P09-FQM-4784 and AYA2010-14844, respectively. TP acknowledges data based on observations made with the NOT, operated on the island of La Palma jointly by Denmark, Finland, Iceland, Norway and Sweden, in the Spanish Observatorio del Roque de los Muchachos of the Instituto de Astrofisica de Canarias.

REFERENCES

Ackermann M. et al., 2011, ApJ, 743, 171
Agudo I. et al., 2006, A&A, 456, 117
Bach U., Krichbaum T. P., Ros W., Britzen S., Tian W. W., Kraus A., Witzel A., Zensus J. A., 2005, A&A, 433, 815
Bach U., Krichbaum T. P., Kraus A., Witzel A., Zensus J. A., 2006, A&A, 452, 83
Beckert T., Fuhrmann L., Cimo G., Krichbaum T. P., Witzel A., Zensus J. A., 2002, in Ros E., Porcas W., Lobanov A. P., Zensus J. A., eds, 6th European VLBI Network Symposium on New Developments in VLBI Science and Technology, Bonn, 2002, p. 79
Bertin E., Arnouts S., 1996, A&AS, 117, 393
Bhat N. D. R., Gupta Y., Rao A. P., 1998, ApJ, 500, 262
Böttcher M. et al., 2005, ApJ, 631, 169
Böttcher M. et al., 2009, ApJ, 694, 174
Breeveld A. A. et al., 2010, MNRAS, 406, 1687
Burrows D. N. et al., 2005, Space Sci. Rev., 120, 165
Camenzind M., Krockenberger M., 1992, A&A, 255, 59
Chandra S., Baliyan K. S., Ganesh S., Joshi U. C., 2011, ApJ, 731, 118
Dondi L., Ghisellini G., 1995, MNRAS, 273, 583
Edelson R. A., Krolik J. H., 1988, ApJ, 333, 646
Fuhrmann L. et al., 2008, A&A, 490, 1019
Gabányi K. É. et al., 2007, A&A, 470, 83
Ghisellini G., Padovani P., Celotti A., Maraschi L., 1993, ApJ, 407, 65
Gopal-Krishna, Wiita P. J., 1992, A&A, 259, 109
Gupta A. C., Banerjee D. P. K., Ashok N. M., Joshi U. C., 2004, A&A, 422, 505
Gupta A. C., Fan J. H., Bai J. M., Wagner S. J., 2008, AJ, 135, 1384
Gupta A. C., Srivastava A. K., Wiita P. J., 2009, ApJ, 690, 216
Hardee P. E., Walker R. C., Gomez J. L., 2005, ApJ, 620, 646
Heidt J., Wagner S. J., 1996, A&A, 305, 42
Kalberla P. M. W., Burton W. B., Hartman D., Arnal E. M., Bajaja E., Morras R., Pöppel W. G. L., 2005, A&A, 440, 775
Kato S., Fukue J., 1980, PASJ, 32, 377
Kolesnikova D. M., Sat L. A., Sokolovsky K. V., Antipin S. V., Samus N. N., 2008, Acta Astron., 58, 279
Kolesnikova D. M., Sat L. A., Sokolovsky K. V., Antipin S. V., Belinskii A. A., Samus' N. N., 2010, Astron. Rep., 54, 1000
Krichbaum T. P., Kraus A., Fuhrmann L., Cimo G., Witzel A., 2002, Publ. Astron. Soc. Aust., 19, 14
Larionov V. M. et al., 2008, A&A, 492, 389
Lehar J., Hewitt J. N., Burke B. F., Roberts D. H., 1992, ApJ, 384, 453
Liu X., Song H.-G., Marchili N., Liu B.-R., Liu J., Krichbaum T. P., Fuhrmann L., Zensus J. A., 2012, A&A, 543, 78
Mangalam A. V., Wiita P. J., 1993, ApJ, 406, 420
Marchili N. et al., 2010, A&A, 509, A47
Marscher A. P., 1987, in Zensus J. A., Pearson T. J., eds, Superluminal Radio Sources. Cambridge Univ. Press, Cambridge, p. 280
Marscher A. P., Gear W. K., 1985, ApJ, 298, 114
Marscher A. P., Gear W. K., Travis J. P., 1992, in Valtaoja E., Valtonen M., eds, Variability of Blazars. Cambridge Univ. Press, Cambridge, p. 85
Marscher A. P. et al., 2008, Nat, 452, 966
Montagni F., Maselli A., Massaro E., Nesci R., Sclavi S., Maesano M., 2006, A&A, 451, 435
Nilsson K., Pursimo T., Sillanpää A., Takalo L. O., Lindfors E., 2008, A&A, 487, L29
Nowak M. A., Wagoner R. V., 1992, ApJ, 393, 697
Ostorero L. et al., 2006, A&A, 451, 797
Pollock J. T., Webb J. R., Azarnia G., 2007, AJ, 133, 487
Poole T. S. et al., 2008, MNRAS, 383, 627
Poon H., Fan J. H., Fu J. N., 2009, ApJS, 185, 511
Qian S.-J., 2008, Chin. J. Astron. Astrophys., 8, 219
Qian S. J., Quirrenbach A., Witzel A., Krichbaum T. P., Hummel C. A., Zensus J. A., 1991, A&A, 241, 15
Qian S.-J., Witzel A., Krichbaum T. P., Wagner S. J., 1995, Chin. J. Astron. Astrophys., 19, 522
Qian S.-J., Li X.-C., Wegner R., Witzel A., Krichbaum T. P., 1996, Chin. J. Astron. Astrophys., 20, 15
Quirrenbach A. et al., 1991, ApJ, 372, L71
Raiteri C. M. et al., 2003, A&A, 402, 151
Raiteri C. M. et al., 2005, A&A, 438, 39
Raiteri C. M. et al., 2007, A&A, 473, 819
Raiteri C. M. et al., 2008a, A&A, 480, 339
Raiteri C. M. et al., 2008b, A&A, 485, L17
Raiteri C. M. et al., 2008c, A&A, 491, 755
Rani B., Wiita P. J., Gupta A. C., 2009, ApJ, 696, 2170
Rani B. et al., 2010a, MNRAS, 404, 1992
Rani B., Gupta A. C., Joshi U. C., Ganesh S., Wiita P. J., 2010b, ApJ, 719, L153
Rani B., Gupta A. C., Joshi U. C., Ganesh S., Wiita P. J., 2011, MNRAS, 413, 2157
Rastorgueva E. A., Wiik K., Savolainen T., Takalo L. O., Valtaoja E., Vetukhnovskaya Y. N., Sokolovsky K. V., 2009, A&A, 494, 5
Rickett B. J., 1990, ARA&A, 28, 561
Roming P. W. A. et al., 2005, Space Sci. Rev., 120, 95
Sagar R., Gopal-Krishna, Mohan V., Pandey A. K., Bhatt B. C., Wagner S. J., 1999, A&AS, 134, 453
Simonetti J. H., Cordes J. M., Heeschen D. S., 1985, ApJ, 296, 46
Smith A. G., Nair A. D., Leacock R. J., Clements S. D., 1993, AJ, 105, 437
Sokolovsky K. V., 2009, Peremennye Zvezdy Prilozhenie, 9, 9
Sokolovsky K., Lebedev A., 2005, in Simon A., Golovin A., eds, 12th Young Scientists' Conf. Astronomy and Space Physics, Kyiv Univ. Press, Kyiv, p. 79
Stalin C. S., Gopal-Krishna, Sagar R., Wiita P. J., Mohan V., Pandey A. K., 2006, MNRAS, 366, 1337
Stetson P. B., 1987, PASP, 99, 191
Svensson R., 1987, MNRAS, 227, 403
Timmer J., König M., 1995, A&A, 300, 707
Urry C. M., Padovani P., 1995, PASP, 107, 803
Valtaoja E., Terasranta H., Urpo S., Nesterov N. S., Lainela M., Valtonen M., 1992, A&A, 254, 71
van der Laan H., 1966, Nat, 211, 1131
Vaughan S., 2005, A&A, 431, 391
Villata M., Raiteri C. M., Lanteri L., Sobrito G., Cavallone M., 1998, A&AS, 130, 305
Villata M. et al., 2000, A&A, 363, 108
Villata M. et al., 2006, A&A, 453, 817
Villata M. et al., 2008, A&A, 481, L79
Villata M. et al., 2009a, A&A, 501, 455
Villata M. et al., 2009b, A&A, 504, L9
Wagner S. J., 1992, in Valtaoja E., Valtonen M., eds, Variability of Blazars. Cambridge Univ. Press, Cambridge, p. 346
Wagner S. J., Witzel A., 1995, ARA&A, 33, 163
Wagner S. J. et al., 1996, AJ, 111, 2187
Walker M. A., 1998, MNRAS, 294, 307
Wu J., Peng B., Zhou X., Ma J., Jiang Z., Chen J., 2005, AJ, 129, 1818
Wu J., Zhou X., Ma J., Wu Z., Jiang Z., Chen J., 2007, AJ, 133, 1599
Zacharias M., Schlickeiser R., 2012, MNRAS, 420, 84
Zhang X.-H., Bao G., 1991, A&A, 246, 21
Zijlstra A. A., van Hoof P. A. M., Perley R. A., 2008, ApJ, 681, 1296

This paper has been typeset from a TEX/LATEX file prepared by the author.